Quasi-Elastic Neutron Scattering Studies on Clay Interlayer-Space Highlighting the Effect of the Cation in Confined Water Dynamics

ARTICLE *in* THE JOURNAL OF PHYSICAL CHEMISTRY C · SEPTEMBER 2008

Impact Factor: 4.77 · DOI: 10.1021/jp803274j

9 AUTHORS, INCLUDING:

Heloisa N Bordallo
University of Copenhagen
151 PUBLICATIONS **1,266** CITATIONS
SEE PROFILE

W. P. Gates
Monash University (Australia)
90 PUBLICATIONS **1,905** CITATIONS
SEE PROFILE

Mark T F Telling
Science and Technology Facilities Council
158 PUBLICATIONS **1,422** CITATIONS
SEE PROFILE

Peter Fouquet
Institut Laue-Langevin
82 PUBLICATIONS **1,039** CITATIONS
SEE PROFILE

Quasi-Elastic Neutron Scattering Studies on Clay Interlayer-Space Highlighting the Effect of the Cation in Confined Water Dynamics

Heloisa N. Bordallo,*,† Laurence P. Aldridge,§,‡ G. Jock Churchman,|| Will P. Gates,⊥,# Mark T. F. Telling,▽ Klaus Kiefer,† Peter Fouquet,○ Tilo Seydel,○ and Simon A. J. Kimber†

Helmholtz-Zentrum Berlin für Materialien and Energie, SF6, Glienicker Strasse, 100, D-14109 Berlin, Germany, IMES, ANSTO and School of Civil and Environmental Engineering, University of New South Wales, NSW Australia, School of Earth and Environmental Sciences, University of Adelaide, SA 5064 Australia, SmecTech Research Consulting, 9 Purtell Street, Bentleigh East, VIC 3165 Australia, Department of Civil Engineering, Monash University, Clayton, VIC 3800 Australia, ISIS Facility, Rutherford Appleton Laboratory, Chilton, Oxon, UK OX11 0QX, and Institut Laue Langevin, 6, rue Jules Horowitz, F-38042 Grenoble Cédex 9, France

Received: August 10, 2007; Revised Manuscript Received: June 27, 2008

It has long been realized that cations play a critical role in the readsorption of water into the interlayer region in clay minerals. To explore possible differences in the water dynamics related to the presence of cations in clays, and to examine the dynamics of its surface water, which plays a prominent role in diffusion of water in clay barriers a comparative study was carried out to highlight differences between water dynamics in montmorillonite and halloysite. Whereas montmorillonite has interlayer cations that interact with interlayer water, and which can rehydrate after dehydration at temperature, halloysite has no interlayer cations. Water is found in both interlayers and on the surface of these clay particles. In this study we show that by combining incoherent inelastic neutron scattering (quasi-elastic and elastic fixed window) and neutron spin echo, it was possible to discriminate the dynamics of surface water (by collapsing the interlayer region by heating and rehydrating the surface layer) from interlayer water. The analysis of the elastic fixed window scans in the temperature range 5−300 K revealed an extension of water dynamics in montmorillonite to lower temperatures than in halloysite. These differences suggested mechanisms that cations (Na^+ in this case) in the interlayer regions facilitate water mobility allowing interlayer water to be readmitted to montmorillonite. Finally it was shown that the occurrence of magnetic fluctuations, caused by the presence of paramagnetic Fe^{3+} ions in the crystalline clay lattice, gave rise to a quasi-elastic contribution that disrupted the evaluation of water diffusion computed from such measurements. Therefore previous estimates of water diffusion coefficients might have been overestimated in recent literature.

Introduction

Interlayer pores of clays provide an ideal environment for the study of confined fluids, and are of relevance to many research subjects, such as cement chemistry,[1] biological interactions,[2] and hydrogeological and petrological processes.[3] Remarkably, smectite-type clays are thought to facilitate the conversion of simple carbon-based molecules to complex ones, which are essential components of the first cell-like systems on Earth. Hence, they can promote the development of diverse organic compounds that may be precursors to the present biomolecules.[4,5]

Montmorillonite, a smectite with a specific composition, is a layered mineral widely found in soils and sedimentary rocks, having an alumino-silicate layer structure (an alumina octahedral sheet bound by two tetrahedral silica sheets with the two combined sheets being about 10 Å thick); see Figure 1a. The interlayer surface of montmorillonite does not contain hydroxyls, as hydroxyls only occur deeper within the structure,[6,7] but does contain oxygens which carry a slight residual charge. However, it is mainly exchangeable cations that balance the negative layer charge residing on the mineral surface. This is the basis for their exchange capacity and swelling properties; i.e., the interlayer regions of montmorillonite tend to expand in the presence of water and aqueous solutions. One interesting feature of interlayer water in montmorillonite is that the water can easily be adsorbed, and clays that have been dried sufficiently e.g., at 0% RH (relative humidity) at room temperature, will exhibit crystalline swelling when exposed to water vapor. For montmorillonite interlayer water, with only Na^+ present as an exchange cation and exposed to an atmosphere at ∼50% RH, there exists only one molecular layer of water in the interlayer, while a similar clay exchanged with Ca^{2+} at a similar humidity would have two molecular layers of water.[8] Thus this system is ideal for studying the effects of confining water with different cations at different concentrations using quasi-elastic neutron scattering (QENS)[2,9−11] neutron spin echo (NSE),[11−13] broadband dielectric spectroscopy,[14,15] and NMR[16] to highlight the complex interactions between water, cations and the surface.

In contrast to montmorillonite, halloysite either contains interlayer water or has contained such water in the past, but

* Corresponding author. Telephone: +49 (0)30 8062 2924. Fax: +49 (0)30 8062 2781. E-mail: bordallo@helmholtz-berlin.de.
† Helmholtz-Zentrum Berlin für Materialien and Energie.
‡ Senior Fellow IMES, ANSTO and School of Civil and Environmental Engineering, University of New South Wales.
§ E-mail: laurie.aldridge@gmail.com.
|| School of Earth and Environmental Sciences, University of Adelaide.
⊥ SmecTech Research Consulting.
Department of Civil Engineering, Monash University.
▽ ISIS Facility, Rutherford Appleton Laboratory.
○ Institut Laue Langevin.

10.1021/jp803274j CCC: $40.75
Published on Web 08/16/2008

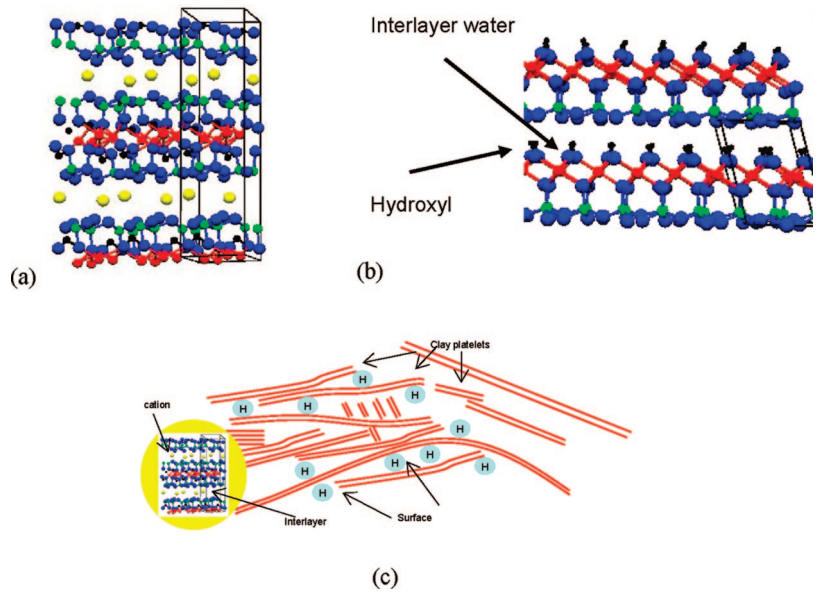

Figure 1. Comparison of the idealized structure of (a) montmorillonite and (b) halloysite showing the positions of the interlayer water and their relation to the hydroxyl bonds. The position of the cations in the interlayer region of montmorillonite is also shown. Interlayer water is confined primarily inside the layers. Note that the hydroxyls in halloysite can directly interact with the interlayer water while the hydroxyls in montmorillonite are separated from the interlayer water. The number of water molecules within the hydration sphere is different, depending on the charge density of the cation involved. Interparticle water resides between clay particles. A schematic view of the interlayer and surface water is shown in (c).

has lost it on drying.[17] Moreover, there are no cations in the interlayer region and so any interlayer water in halloysite is not associated with cations, but instead with the interlayer surfaces only. Thus halloysite uniquely allows us to examine the effect of interaction of water confined within an interlayer space as a monolayer without any interaction with cations. Halloysite, Figure 1b, has a 1:1 aluminosilicate structure (composed of one silica tetrahedral sheet bonded to one alumina octahedral sheet).[18] One surface within the interlayer of halloysite presents hydroxyls groups which can readily form H-bonds with interlayer water. Finally, in halloysite, it is possible to irreversibly remove interlayer water simply by heating, allowing the behavior of surface water in clay to be contrasted to the interlayer water.

The diffusion of water through clays is also of fundamental interest to technologists involved in nuclear waste repositories.[19] However of the two types of water found in clay it is the surface (or interparticle, see Figure 1c) rather than the interlayer water that dominates water diffusion.[20] Hence it is of great consequence for the effectiveness of clay barriers to elucidate the dynamics of the surface water. Within halloysite this is straightforward—after the clay is dry, it will not readsorb water into the interlayer and so any readsorbed water will be surface water adsorbed onto the outside of clay particles. However with montmorillonites it is more difficult to examine water associated specifically only with the clay surface. Here, we have used the so-called *reduced charge montmorillonites*[21] to compare the different types of water. The *reduced charge montmorillonites* are prepared by saturating the interlayer exchange sites of the clay with Li^+ and then heating the clay to 250 °C. As a result of this treatment, Li cations migrate from the interlayer to vacant sites within the montmorillonite structure, thereby neutralizing a portion of the permanent layer charge. It is well established that such treatment results in a collapse of the interlayer space and the loss of interlayer water.[22] Thus, in these samples there will be predominantly surface water.

The present study aims, in particular, at elucidating the role of the cations in controlling the dynamics of interlayer water in clays. Previous infrared studies in montmorillonite[23,24] have shown that water molecules residing close to the surface are strongly influenced by the type of exchangeable cation present on the clay as well as by the overall water content. For instance, for water contents $<6H_2O$ molecules per exchangeable cation, the H−O−H bending mode of H_2O shifts to a lower frequency, while the positions of the asymmetric and symmetric OH-stretching modes of adsorbed water shift to higher energies. These observations indicate that H_2O molecules adsorbed to the clay interlayer surface at low-water content are less H-bonded than in bulk H_2O. The reversible transport of water into and out from the interlayer is facilitated by these cations as is highlighted by the fact that clays lacking interlayer cations (i.e., talc, pyrophyllite, and *reduced charge montmorillonite*) do not have hydrated interlayers.

While many workers have examined the quasi-elastic (QE) component of the time-of-flight (ToF) spectra of water in clays this is the first time to our knowledge that any systematic study has been carried out contrasting the QE response of interlayer water, which has no cations present, to the spectra of clay having water in interlayer regions of similar size and with substantial amounts of cations present. Preceding studies[25] have indicated that it is the presence of the cations that allows the return of water to the interlayer region so insights to this bonding may give a new insight into the mechanisms of water adsorbed into the interlayer region.

The interlayer surfaces of halloysite and montmorillonite/*reduced charge montmorillonite* are different—even without considering the interlayer cations. Halloysite contains both siloxane and aluminous hydroxyls on either side of the interlayer, whereas the montmorillonite contains only siloxanes. Thus the water in halloysite can be potentially H-bonded more effectively than in montmorillonite or *reduced charge montmorillonite*. When cations are present, as in montmorillonite, the hydration energies of the interlayer cation impact strongly on the H-bonding that occurs within the interlayer, the greater water content the greater H-bonding. Without cations, as in the *reduced charge montmorillonite*, the H-bonding is only to the

TABLE 1: Description of the Different Clays Measured in This Work[a]

sample	clay type	% RH	heated	interlayer water	surface water	composition[b]
1	halloysite	98		yes	yes	$Si_2Al_2O_5(OH)_4$ [2.0] (0.6) H_2O
2	halloysite	55		yes	yes	$Si_2Al_2O_5(OH)_4$ [2.0] (0.3) H_2O
3	halloysite	55	yes	no	yes	$Si_2Al_2O_5(OH)_4$ [0] (0.3) H_2O
4	montmorillonite	55		yes	yes	$Na_{0.9}\{Si_{7.7}Al_{0.3}\}\{Al_3Fe_{0.4}Mg_{0.6}\}O_{20}(OH)_4$ [6.0] (0.3) H_2O
5	montmorillonite	55	yes	no	yes	$\{Si_{7.7}Al_{0.3}\}\{Al_3Fe_{0.4}Mg_{0.6}Li_{0.9}\}O_{20}(OH)_4$ [0] (0.3) H_2O

[a] The Te Puke halloysite comes from the same deposit as the sample used by Churchman et al.,[26] and the Jelšový Potok montmorillonite from that used by Komadel et al.[27] Note that water split between the surface and interlayer is based on estimates. [b] [ ] denotes interlayer water; ( ) denotes surface water.

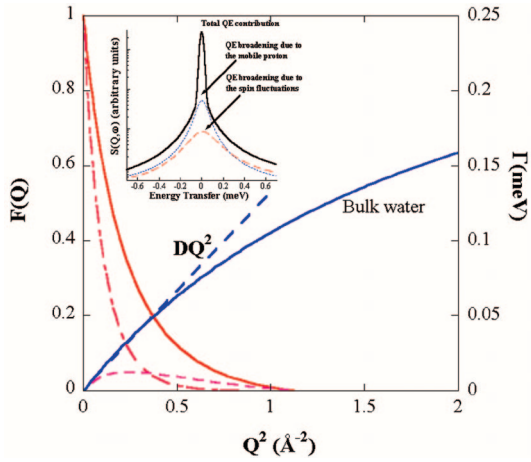

Figure 2. Magnetic form factor $F(Q)$ describing the Q-dependence of the scattering amplitude from Fe^{3+}. $F(Q)$ may be calculated using $\langle j_0 \rangle$ (full line) and $\langle j_2 \rangle$ (dotted line), from the relationship $F(Q) = \langle j_0 \rangle(Q) + (1 - 2/g)\langle j_2 \rangle(Q)$ from the values given in ref 36. The dotted point line represents $\langle j_0 \rangle^2$. Inset: Line width (hwhm) as a function of Q^2 of the QE component for bulk water, using 5.1 Å neutrons, with $\Delta E = 100$ μeV. The line represents a fit to the data using the Singwi and Sjölander[49] model and the dotted line shows the DQ^2 dependence. The insert shows a schematic $S(Q,\omega)$ for a system containing both magnetic and mobile proton contributions at low Q-values.

residual charges on the siloxane oxygens, which will be significantly less than in either halloysite or montmorillonite.

Materials and Methods

Clay Samples. Two different types of clays were used: a Te Puke halloysite from the same deposit as the sample used by Churchman et al.[26] and a Jelšový Potok montmorillonite from that used by Komadel et al.[27] As indicated in Table 1, five samples of the clays were prepared for QENS measurement: (1) original (water saturated) halloysite after equilibration with an atmosphere of 98% RH; (2) original halloysite after equilibration with an atmosphere of 55% RH; (3) halloysite heated to 250 °C and then equilibrated at an RH of 55% RH; (4) a sample of montmorillonite equilibrated with an atmosphere of 55% RH; (5) the *reduced charge montmorillonite* after equilibration with an atmosphere of 55% RH. Before exposure to 55% RH, all samples were pretreated and prepared using standard methods so that the particles were less than 2 μm and were equilibrated (after Na^+ exchange) at 55% RH. The presence of different hydrated phases of halloysite and montmorillonite was monitored by X-ray diffraction.[8,26] The RH was controlled by saturated solutions of $Mg(NO_3)_2 \cdot 6H_2$ O and $CuSO_4 \cdot 5H_2O$. The *reduced charge montmorillonite* was exchanged with Li^+ and then heated at 250 °C for 12 h and then resaturated with Na^+ followed by equilibration at 55% RH. This procedure removes cations from the interlayer and ensured that the same cation, viz. Na^+ would be on the surface of the clay of the two montmorillonite samples. Note that sample 3 is denoted halloysite without interlayer water and sample 5 is denoted montmorillonite without interlayer water in the subsequent figures and tables.

Neutron Scattering Techniques. Quasi-elastic neutron scattering spectra were measured using the ToF inverted geometry crystal analyzer spectrometer OSIRIS[28] situated on the N6(B) beam line located at ISIS, U.K. Elastic energy resolutions ΔE of 25 or 100 μeV (at full width at half-maximum (fwhm)) within an angular range of $11° < \theta < 155°$ were achieved by using the two analyzing reflections of the pyrolytic graphite analysers, PG002 and PG004. For the QENS data analysis, after removing Bragg peaks, the spectra were grouped to obtain eight constant angle spectra, resulting in a wave vector transfer range of 0.08 $Å^{-1} < Q < 2.9$ $Å^{-1}$, where $Q = (4\pi/\lambda)\sin(2\theta/2)$ is the magnitude of the wave vector transfer, 2θ the scattering angle, and λ the incident neutron wavelength.

To obtain an overall view of water dynamics in the different clays, the EFW (elastic fixed window) technique in the temperature range 5−300 K was used, enabling the analysis of the Q-dependence of the structure factor,[29] $S_E(Q,\omega=0)$ Similarly to the X-ray Debye−Waller effect, the normalized elastic scattering, $[S_E(Q,0)(T)/S_E(Q,0)(T=5\text{ K})]$ can be related to the Debye−Waller factor:[30]

$$S_E(Q,\omega\approx 0) = \exp(-\langle u(T)^2\rangle Q^2/3) \quad (1)$$

where $\langle u(T)^2\rangle$ is the mean square displacement of the atoms around the equilibrium positions of the H atoms. By focusing on the analysis of the QE region, we can access different correlation times associated with the water mobility.

For the EFW measurements we used the IN10 backscattering spectrometer at the Institute Max von Laue-Paul Langevin, France[31] as well as the OSIRIS ToF spectrometer. The backscattering spectrometer was used with unpolished Si (111) crystals, with an elastic energy resolution (ΔE) of 1 μeV (fwhm). During the ToF experiment, ΔE of 25 or 100 μeV (fwhm) were used.

The samples were confined in a flat volume and sealed between aluminum plates. The angle between the plane of the sample and the incident neutron beam was 135°. Using this orientation the higher detectors have to be discarded. All spectra were corrected by normalization of the detectors with vanadium and subtraction of the empty cell scattering using standard routines available at ISIS and ILL.

Measurements of the intermediate scattering function $S(q,t)$ on montmorillonite RH = 55% with one water layer were performed on IN11 in the time range of 5 ps to 1.3 ns, using an incident neutron wavelength of 5.5 Å and thus providing a measurement range which extends over 2.5 orders of magnitude in time. The data were collected for various temperatures between 2 and 300 K. Initially, the data were corrected for

instrumental spin−echo resolution by normalizing each scan to the reference scan of an elastically scattering TiZr sample with the same dimensions as the sample. The sample was then cooled to 2 K to verify the validity of this resolution correction.

As the transmission values were kept around 0.9 for both ToF and NSE experiments, multiple scattering corrections were not applied.

Magnetic Measurements. Direct comparison[11,32] of diffusion coefficients of water in the interlayer of natural montmorillonite determined using NSE and ToF did in some cases give significantly different values, however such differences were not encountered while studying synthetic hectorite clay.[33] Hence it was of great interest to determine if there were any other factors that might effect the evaluation of water diffusion obtained using such techniques. The presence of transition metal ions in minerals implies the presence of a magnetic moment due their incompletely filled 3d-shells.[34,35] The most common transition metal ion is iron whose abundance in the crust is approximately 40 times that of all the other magnetic elements together. The magnetic properties of minerals and clay minerals are therefore essentially due to the iron they contain, either as iron oxy-hydroxide impurities or, as is found in this case, by iron incorporated into the layer structure. As illustrated in Figure 2, the magnetic neutron scattering cross section of a single Fe^{3+} ion[36] and the component characterizing the scattering law for water diffusion contribute significantly to the QE signal. Therefore, the common presence of Fe_2O_3 incorporated in clay,[18,37] (chemical analysis and charge balance calculation in many halloysites reveals the existence of significant amounts of iron incorporated within the aluminosilicate layer—up to 12.8 wt % of Fe_2O_3), may give rise to magnetic contributions that can not be neglected in our studies. To evaluate such a contribution, magnetic measurements were made using a vibrating sample magnetometer (Quantum Design PPMS) and SQUID magnetometer (Quantum Design MPMS), and the temperature dependence of the susceptibility deduced. A typical sample mass was 100 mg.

Results

Results obtained from the EFW measurements as a function of temperature using different energy resolutions on the unheated clays are presented in Figure 3. The data plotted in this figure have a summed Q-range taken between 0.4 and 1 Å and were normalized to unity at the lowest temperature. As expected $S_E(Q,\omega=0)$ decreases with increasing temperature; however, as indicated by the arrows, inflection points are clearly observed. If we assume that we are dealing with true E and QE scattering, the elastic incoherent structure factor is evaluated using

$$A_o(Q) = \int S_E \, d\omega / (\int S_E \, d\omega + \int S_{QE} \, d\omega) \qquad (2)$$

The rapid increase in the QE line width indicates that localized or translational diffusive motions are activated. Interestingly, the $S_E(Q,\omega=0)$ obtained from the three resolutions evolves as a function of temperature in a very distinct manner. Therefore we can conclude that (i) the dynamic transition depends heavily upon the time window of the probed water motion and that, (ii) in order to explain the significant differences between the unlocking temperatures of the dynamics, there have to be significant differences in the dynamic processes in halloysite and montmorillonite. It should be noted that the difference between the lowest values of ratios of S_E in Figure 3 (~0.2 for montmorillonite and ~0.5 for halloysite) can be accounted for by the differences in the ratio of hydrogen bound as hydroxyls to hydrogen in the water shown in Table 1. For instance, in the case of natural montmorillonite a constant elastic background was observed during the NSE experiments, which is absent in the hectorite that contains no structural hydrogen.[33] Moreover, as was observed in cement pastes,[38,39] such incoherent elastic scattering contribution suggests that in the montmorillonite a long-range translational diffusion of the protons may be observed as well. Furthermore, there might be proton exchange between hydrogen bound as hydroxyls to hydrogen in the water.

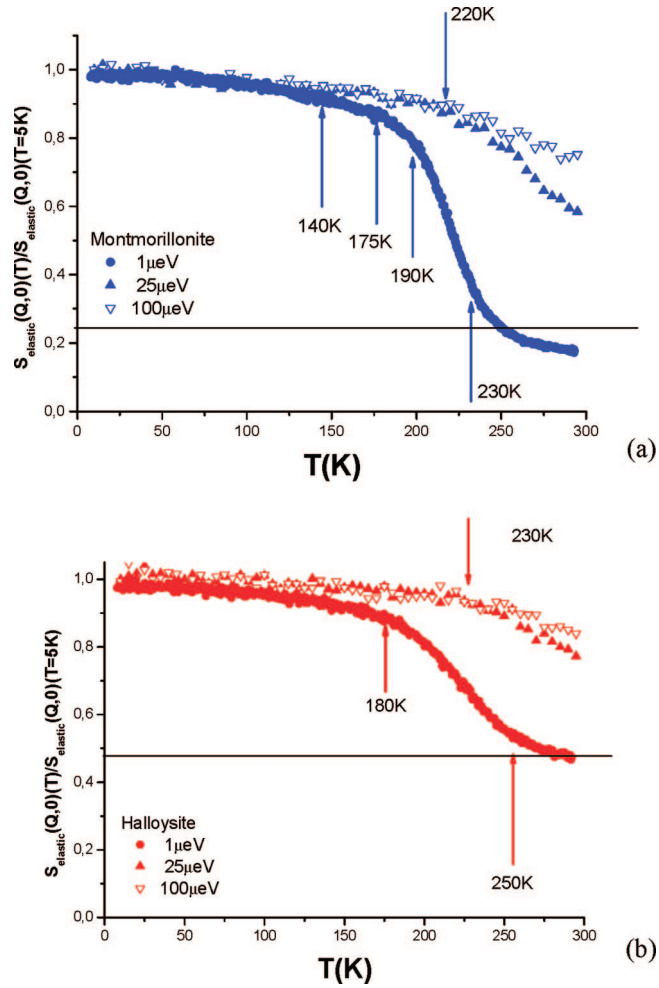

Figure 3. Comparison between the normalized intensity $S(Q,0)(T)/S(Q,0)(T=5\text{ K})$ from three different energy resolutions, 100, 28, and 1 μeV, as a function of temperature between montmorillonite (a) and halloysite (b). The data plotted in this figure have Q values ranging between 0.4 and 1Å. The horizontal lines indicate the ratio of hydrogen in hydroxyls to water based on the data given in Table 1. The arrows indicate where $\langle u^2 \rangle$ deviates from the harmonic behavior (linear increase on a given temperature range).

We can analyze the differences between rotational and the translational contributions to the diffusive motion by assuming that $S_E(Q,\omega=0)$ is separated in two regions,[40,41] with a low Q-range $\langle Q \rangle \leq 1$ Å^{-1} associated with the long-range translational diffusion ($\langle$trans$\rangle$), and a higher Q range $\langle Q \rangle \geq 2-3$ Å^{-1} related to local rotational dynamics ($\langle$rot$\rangle$).

For the unheated clays, the measured $S_E(Q,\omega=0)(T)$, normalized to the extrapolated intensity at 5 K are shown for three $\langle Q \rangle$ values in Figure 4, parts a and b. Following the Debye model $\ln((I_\infty^{DWF}(T) \sim -T)$, within a certain temperature range, the intensity decreases with temperature; i.e., the normalized elastic scattering can be fitted by a straight line. However, as illustrated

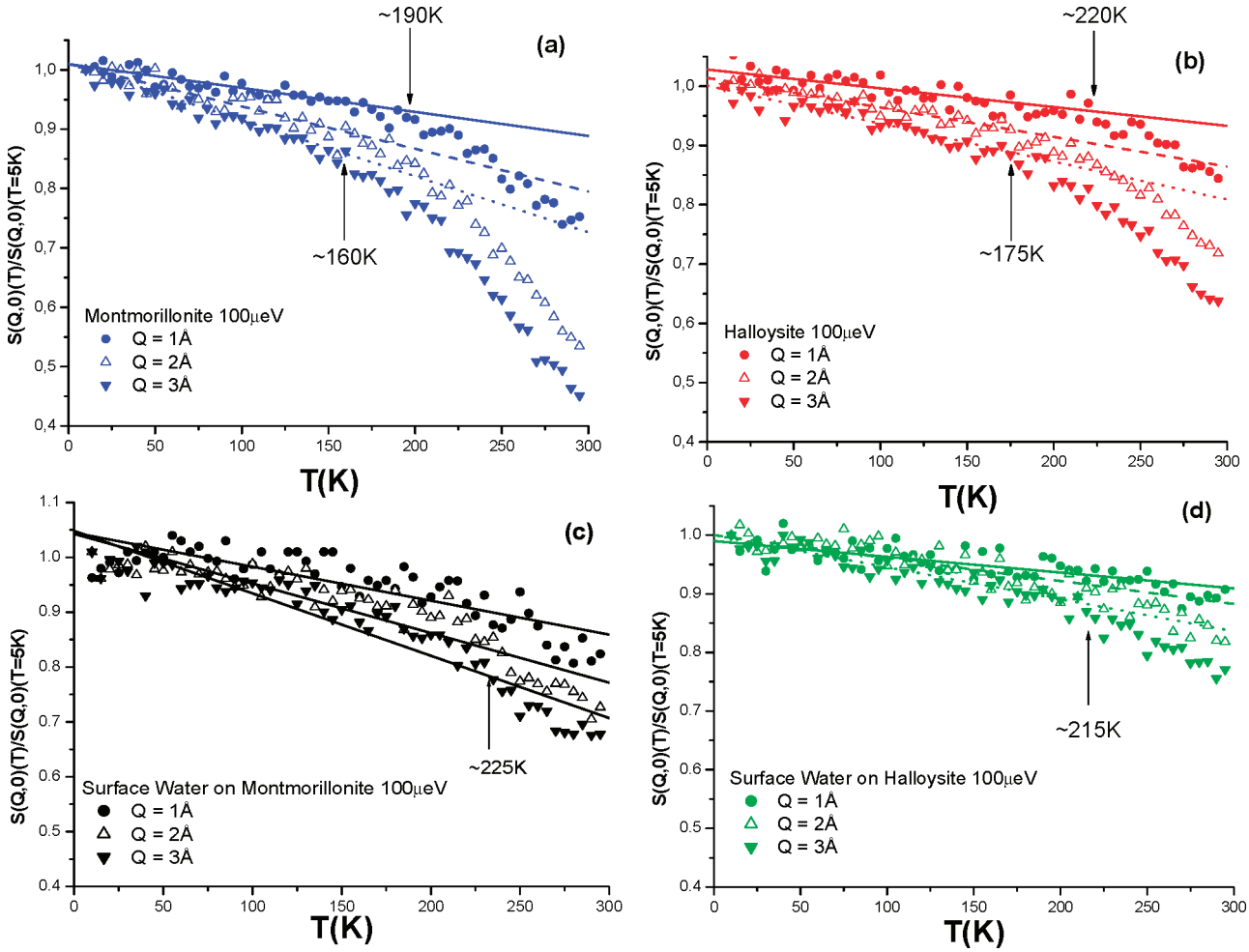

Figure 4. A comparison between the normalized intensity $S(Q, 0)(T)/S(Q,0)(T=5\text{ K})$ of (a) montmorillonite (b) halloysite, (c) surface water on montmorillonite, and (d) surface water on halloysite. Data obtained on ORISIS with $\Delta E = 100\ \mu$eV.

in Figure 4a for montmorillonite there is an anomalous decrease of the elastic intensity at about 190 K for ⟨trans⟩, and at about 160 K for ⟨rot⟩ that can be explained by the onset of some type of diffusive motion that is faster than the instrumental time resolution of 10^{-10} s and now visible with the resolution of the spectrometer. For halloysite, Figure 4b, the crossover temperatures are higher, 220 K for ⟨trans⟩, and 175 K for ⟨rot⟩, which suggests that for each sample the scattering function broadens due to the occurrence of QE components imposed by individual physical parameters of the diffusive motions in a characteristic temperature range.

Considering that small cations such as Na^+ are designated as structure-making cations, because they strongly interact with water molecules,[42] as a result the original H bonds are broken. This could cause an organization of the water molecules around the cation, leading to the formation of a transient network of hydrogen bonded water molecules. However, from the EFW results it can be suggested that the interlayer cations facilitate the activation of water dynamics at a lower temperature in interlayer water in montmorillonite compared to halloysite. As has been very recently shown by Kamitakahara and Wada,[43] a direct comparison of QENS data on hydrated silica-based materials, bulk water, and aqueous solutions, indicated that the presence of ions and charged silicate surfaces have a dominant effect in determining the behavior of the diffusive motion of water molecules. The results presented here substantially support this finding: the montmorillonite used in our study contains sufficient octahedrally bound magnesium, as well as tetrahedrally bound aluminum, to display elevated surface charges, and thus contains more sodium than the halloysite. The occurrence of tetrahedral aluminum ensures this difference even when the montmorillonite is *charge reduced*.

On the other hand if it is the interlayer structure that plays the major role in governing the mobility of water molecules, it will be reflected in the values of the diffusion constants.[44] As discussed above, the interlayer surface of halloysite and montmorillonite are different—even without considering the interlayer cations. Thus if such a geometrical arrangement plays a more significant role compared to the presence of the cation, the average number of hydrogen bonds between the water molecules will be reduced and the average diffusional motion of confined water will be slowed down; i.e., $D_{\text{halloysite}} < D_{\text{montmorillonite}}$. As we show in the next section this is not true, supporting the hypothesis that it is the interlayer cations that play the major role in governing the mobility of interlayer water.

The large scattering cross section of H relative to other atoms in clays makes QENS ideally suited for studies of water mobility. Moreover analysis of the QE scattering provides information about both the time-scale and the geometry of the motion.[2,9,11−13,30,38] Therefore QENS experiments were performed and are presented in the next section.

Differences between the water mobility on clay particle surfaces should be reflected by the measured $S_E(Q,\omega=0)(T)$ on the heated clays. Differences in the unlocking temperatures would indicate differences in the water interactions with the chemistry of the outer surface. Thus results of surface water

obtained from the heated montmorillonite (sample 5) and the heated halloysite (sample 3), Figure 4, parts c and d, respectively, show that the activation of water dynamics only occurs at much higher temperatures then that of the interlayer water, about 225 and 215 K, respectively. Furthermore, the lack of Q-dependence indicates that only constrained motions independent of length scale are taking place. This is characteristic of water mobility close to an interface such as the outer monolayer found here.

Distinctive Dynamical Aspects of Each Clay Obtained from the Quasi-Elastic Measurements. Since the hydroxyl group can be considered to be either immobile or moving too slowly for the OSIRIS time-window, it contributes to the elastic part of the signal and so only the dynamics of water is expected to be observed in our measurements.[45] By focusing on the analysis of the quasi-elastic (QE) region of the inelastic incoherent neutron scattering spectrum obtained on OSIRIS from the two data sets with different energy resolutions and covering different energy transfer ranges, we can access different correlation times associated with the water mobility in the various clay samples. Although protons will be involved not only in rotation around the center of mass of the water molecule, but also in long-range translational motions that occur on two different time scales,[46,47] the simplest analytical model to describe the diffusion of water assumes decoupled translational and rotational motions:[47]

$$S_m(Q,\omega) = e^{-\langle u^2\rangle Q^2/3} T(Q,\omega) \otimes R(Q,\omega) \qquad (3)$$

The first term is the Debye−Waller factor that gives the probability for a neutron to be elastically (or quasi-elastically) scattered. $T(Q,\omega)$ denotes the contribution from the translational motion of the molecule and $R(Q,\omega)$ the contribution for the low-frequency rotational motion. For the present experimental Q-range a random rotational motion on the surface of a sphere, $R(Q,\omega)$ is given by the first four terms of the Sears expansion[48]

$$R(Q,\omega) = j_0^2(Qa)\delta(\omega) + \frac{1}{\pi}\sum_{l=1}^{4}(2l+1)j_l^2(Qa)\frac{l(l+1)D_r}{(l(l+1)D_r)^2+\omega^2} \qquad (4)$$

where a is the radius of gyration taken as the O−H distance in a water molecule (0.98 Å). D_r is the rotational diffusion constant and j_l are the spherical Bessel functions. The rotational diffusion is characterized by a relaxation time $\tau_r = {}^1/_6 D_r$.

The translational component, $T(Q,\omega)$ is commonly modeled by a Lorentzian with half-width at half-maximum $\Gamma_T(Q)$,[30]

$$T(Q,\omega) = \frac{1}{\pi}\frac{\Gamma_T(Q)}{\Gamma_T^2(Q)+\omega^2} \qquad (5)$$

Considering a random diffusion process, the variation of Γ_T vs Q can be approximated by the model of Singwi and Sjölander[49]

$$\Gamma_T(Q) = \frac{D_t Q^2}{1 + D_t Q^2 \tau_0} \quad \text{and} \quad D_t = \frac{L^2}{6\tau_0} \qquad (6)$$

where D_t is the self-diffusion coefficient, τ_0 is the average residence time between jumps, and L is the mean jump distance.

In recent years, several groups have applied the so-called "relaxing cage model" (RCM) as an alternative method for analyzing high-resolution QENS data.[50−52] In this approximation, the dynamics are dominated by a "cage" effect, thus revealing correlation between the translational diffusion and the rotation of the water molecules, and implying the cessation of the isotropic nature of the diffusion. In such a framework the water molecule is localized by interactions with its neighbors and with the interface, implying a very complex but accurate description of water diffusion. It is essential to bear in mind that this model is expected to be valid only for the lower range of Q.

In this case, the dynamics may be described as[51]

$$T_{RCM}(Q,\omega) = \frac{A(Q)}{\pi}\int_0^\infty \cos(\omega t)\exp\left(-\left(\frac{t}{\tau}\right)^\beta\right) dt \qquad (7)$$

$A(Q)$ is the elastic structure factor (EISF). τ and β are functions of Q. τ represents the characteristic time for the structural relaxation. The variation of β from unity indicates that the system deviates from the "decoupling approximation" behavior.

Keeping in mind that the time scale at which the correlation functions are probed is determined by the energy resolution ΔE of the spectrometer, different time domains are accessible by employing various energy resolutions.

(a) PG (004) Data on Halloysite 55% RH, Halloysite 98% RH and Montmorillonite 55% RH: Using the Diffusion Model To Describe the Water Dynamics. To analyze the PG (004) data ($\Delta E = 100$ μeV) we used the Singwi and Sjölander diffusion model described by eq 6 to extract the parameters D, L, and τ from the half-width at half-maximum (Γ, hwmh)[53] of the experimental scattering peak. From the unconstrained variation of $\Gamma_T(Q)$ as a function of momentum transfer, and as shown in Figure 5, we find the expected Q-dependence of the diffusion model. The fit parameters, characterizing the fast water motion, are given in Table 2.

(b) PG (002) data on Halloysite 55% RH, Halloysite 98% RH, and Montmorillonite 55% RH: Using the RCM Model To Describe the Water Dynamics. The RCM model was used[54] to estimate the diffusion coefficient from the high resolution data (PG002, 25 μeV). The momentum transfer (Q), $\hbar Q = \hbar k_i - \hbar k_f$, carries information about spatial distance, while the energy change $\hbar\omega = \hbar E_i - \hbar E_f$, provides information on the time scale of the motion (as time t and the energy $\hbar\omega$ are inversely proportional). As described above, the RCM model replaces the choice of several Lorentzians with a single function having the shape of a stretched exponential. Figure 6 shows the fit result using this model for the spectra obtained from montmorillonite 55% RH at $Q = 0.82$ Å^{-1}. The evolution of the two parameters, Γ (or reciprocal relaxation time) and β, as a function of Q is shown in Figure 7. As seen in Figure 7a, the structural relaxation has a power-law dependence on Q. From Figure 7b, it is clear that β appears to decrease with increasing Q. Thus one can infer that the structural relaxation can be described by a power-law dependence in Q, $\bar{\tau} \propto Q^{-\gamma}$. In view of the better data quality for the halloysite 98% RH, we fitted the average relaxation time dependence in Q, as shown in the log−log plot in Figure 7c. Once again at high Q values the decoupling model is not valid (i.e., both long-range and shorter-range processes are correlated); however, for $Q \leq 1.1$ Å, the exponent γ is close to 2, and approaches the long-range translational diffusion case.[46,50,51] From these assumptions, we can roughly estimate an average diffusion coefficient, $\bar{\tau} = 1/\bar{D}Q^2$. Considering that, for $Q = 0.3$ Å^{-1} and $\bar{\tau} = 620$ ps, we can estimate $\bar{D}$ to be 0.2×10^{-9} m^2/s. It is evident that to achieve a correct value of diffusion coefficients it is crucial to have access to a large number of points at small Q values.

The apparent diffusion constants, D, and the apparent residence time, τ, values obtained from the analysis of our data are similar to results obtained either experimentally (using

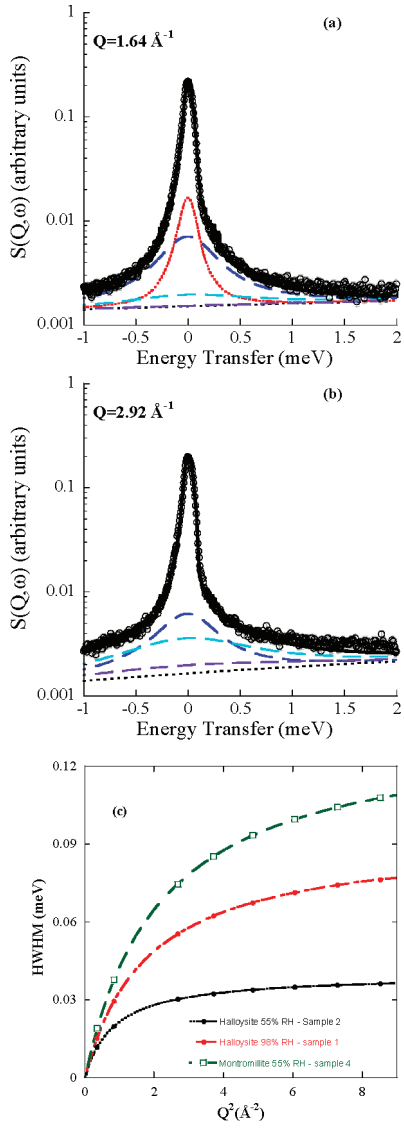

Figure 5. (a and b) Experimental spectra (○) at selected Q values for the montmorillonite 55% RH, ΔE =100 μeV, together with the best fit (solid line) and the QE components (dotted lines represents the translational component and the long dashed lines represents the first three terms of the Sears expansion used to describe the rotational motion. The background is also shown (short dashed line). (c) Linewidth (HWHM) of the translational Lorentzian $\Gamma_T(Q)$ of eq 4) as a function of Q^2 of the QE component for water contained in the clays, using the PG004, with ΔE = 100 μeV. The solid lines are fit to the data using the jump diffusion model giving the diffusion constants values and average residence times listed in Table 1.

QENS) or by molecular dynamics for clays at room temperature, as well as for synthetic layered materials with more well-defined structural chemistry. These values are all in the range (0.03 −1.2) *.10^{-9}m^2/s).[9,10,55−61]

(c) PG (002) Data on Halloysite or Montmorillonite with Surface Water (Samples 3 and 5). In samples 1, 2, and 4 interlayer and surface water are both present. Hence the line widths from which the diffusion constants given in Table 2 are calculated include both components, i.e., $\Gamma_{watert} = \Gamma_{interlayer} + \Gamma_{surface}$. In order to obtain values of $\Gamma_{surface}$ both samples 3 and 5, where water adsorption is expected to occur only on the external surface of the clay, were analyzed. However as the structure factor representing the surface water is much smaller than that of interlayer water plus the consideration that surface water should have different mobility depending on the number

TABLE 2: Parameters Characterizing the Rotational and Translational Motion of Water in the Various Clays Studied Using OSIRIS[a]

sample	τ_r (ps) (fixed)	L (Å)	τ_0 (ps)	$D_{apparent}$ (10^{-9}m^2/s)
bulk water[46,47]	1.07	1.53	1.57 ± 0.12	2.49 ± 0.07
halloysite 55% RH	1.07	2.6 ± 0.1	16.5 ± 0.5	0.7 ± 0.2
halloysite 98% RH	1.07	1.8 ± 0.2	7.1 ± 0.6	
fast[b]				0.8 ± 0.1
slow[b]				∼0.2
montmorillonite 55% RH	1.07	1.6 ± 0.2	4.9 ± 0.4	0.9 ± 0.1
surface water halloysite	1.07	1.25	1.24 ± 0.09	2.1 ± 0.5
surface water montmorillonite	1.07	1.28	1.15 ± 0.09	2.4 ± 0.4

[a] Values of bulk water are given for comparison. τ_R characterizes the rotational diffusion, L gives the mean jump distance, τ_0 is the average residence time between jumps, and D is the self-diffusion coefficient. [b] As described in the text in view of the better data quality for the halloysite 98% RH an average diffusion coefficient, $\bar{\tau}$. Therefore a slow translational motion of water molecules was obtained from the analysis of PG[002] data, whereas a faster translational motion was accessed by from the fit of PG[004] data using the model of Singwi and Sjölander.[49]

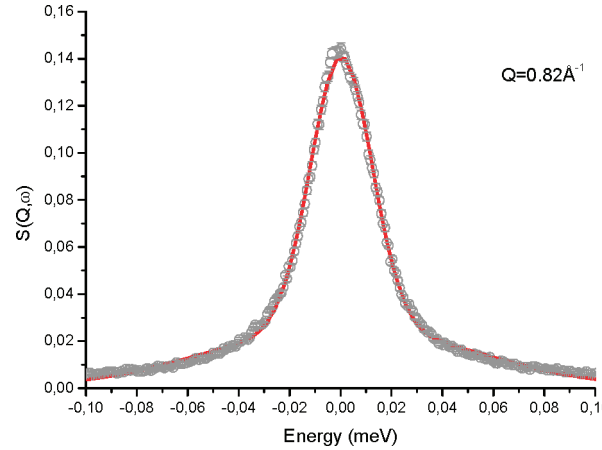

Figure 6. Experimental spectrum (○) at Q = 0.82 Å^{-1} for the montmorillonite 55% RH, ΔE =25 μeV, together with the best fit (solid line). The solid lines are fit to the data using the RCM model.

of layers of surface water implies that the determination of $\Gamma_{surface}$ is difficult. It should be remembered that the EFW results indicate that the surface water gave no significant translation motions. The spectra were fitted using a phenomenological expression

$$S_m(Q,\omega) = F\{[A_0\delta(\omega) + A_1L_1(\Gamma_1,\omega)] \otimes F(\omega)\} + B \quad (8)$$

where F is the scaling factor, A_1 is the structure factor, A_0 represents the EISF, $L_1(\Gamma_1,\omega)$ is the Lorentzian function having the half-widths at half-maxima (HWHM) Γ_1 and $F(\omega)$ is the experimental resolution function. The flat background term, B, represents the inelastic contribution. Figure 8 shows the evolution of the Γ as a function of Q^2. Applying eq 6 to fit Γ vs Q^2 leads to diffusion coefficients D_t = 2.1 and 2.4 × 10^{-9} m^2/s and residence times τ_0 = 1.2 ps in halloysite and montmorillonite, respectively. It should be noted that this analysis indicates that a small amount of "bulk water" is present in the surface dominating the QENS signal and hinders the full analysis of $\Gamma_{surface}$ in the monolayer.

The use of new instruments like TOFTOF at FRMII that combine both high flux and low background should make the full analysis of $\Gamma_{surface}$ possible, if allowance can be made for the paramagnetic scattering observed in natural clays that is discussed in the next section.

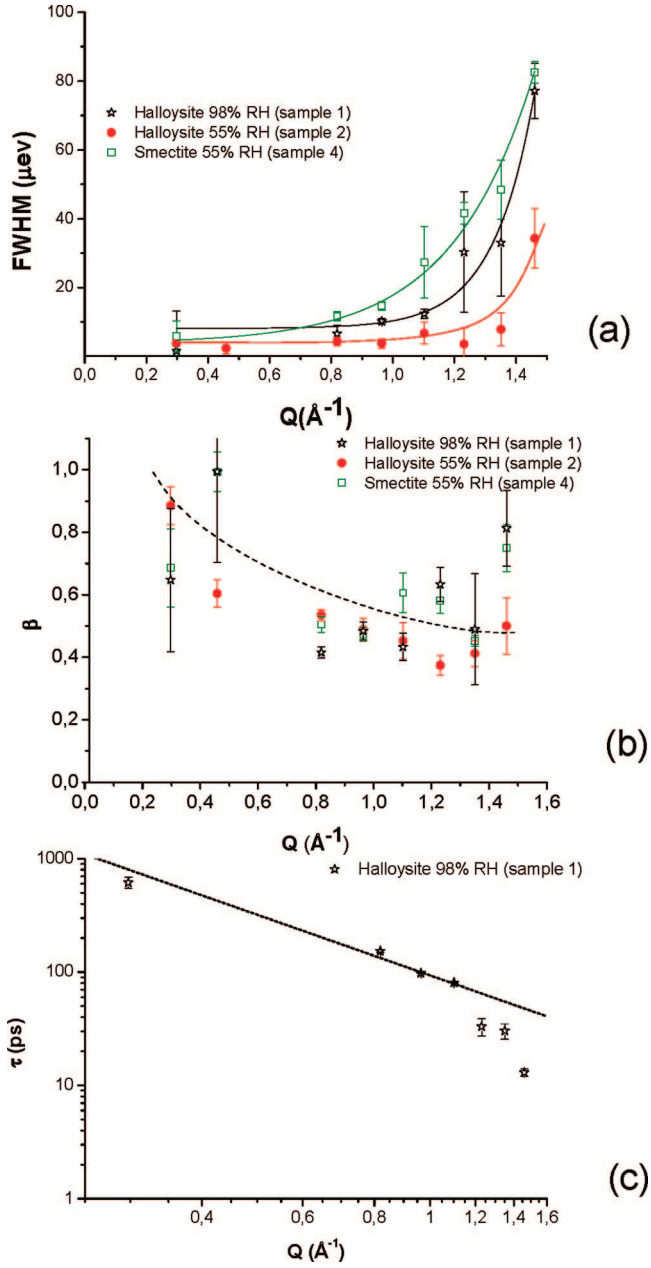

Figure 7. (a) Q dependence of the quasi-stretched exponential width in μeV measured with the PG002 setup (ΔE = 25 μeV) for (*) halloysite 98% (sample 1), (●) halloysite 55% (sample 2), and (□) montmorillonite 55% (sample 4). It can be clearly observed that as Q increases the scattering associated to rotational motions becomes more dominant. (b) Q dependence of the stretch exponent β showing a decrease with increasing Q. The line is a guide to the eyes. (c) Average relaxation time τ for the halloysite 98% RH plotted vs Q in log−log scales. The slope is close to 2, allowing for the use of a simple diffusion approximation and estimation of an average diffusion constants value $\bar{D} = 0.2 \times 10^{-9}$ m²/s.

In this study the surface water of the clay particles, as indicated in the introduction should be confined to a monolayer. Because water diffusion through clay barriers is determined by the mobility of this water further studies of this surface water are planned at concentrations higher than a monolayer.

Magnetic Fluctuation Contributions Evidenced by Neutron Spin−Echo and Magnetic Susceptibility Measurements. ***Neutron Spin Echo.*** The neutron spin−echo (NSE) method measures the intermediate scattering function $S(Q, t)$, which is defined by the following equation as a function of the wave vector Q and Fourier time t.

$$S(Q,t) = N^{-1}\sum_{k,l}\langle \exp^{iQ\cdot r_k(t)} \exp^{iQ\cdot r_l(0)}\rangle \quad (9)$$

where N is the number density, $r_{k,l}$ is the position of the scattering atom at time t, and Q is the wave vector. Through a time frequency Fourier transform of $S(Q,t)$ one gets the usual scattering law, $S(Q,\omega)$. In addition, the NSE signal is sensitive to the spin−spin interaction of the probing neutron with the sample and can identify coherent, incoherent and magnetic scattering. Magnetic and incoherent scattering will lead to a 180° flip of the neutron spin, which will manifest itself in a 180° change in the phase of the NSE signal. This phase change will show up as a negative polarization in the $S(Q,t)$ curve. Data analysis yielded $S(Q,t)/S(Q,0)$ for three different q-values corresponding to Q = 0.25, 0.37, and 0.6 Å, and for Fourier times $0.03 < t < 1$ ns. As a first phenomenological description, we may use Kohlrausch−Williams−Watts (KWW) or stretched exponential functions to parametrize the data:[12]

$$S(Q,t)/S(Q,0) = A\exp(-t/\tau)^{\beta} + B \quad (10)$$

τ is the typical relaxation time, β a stretching parameter, and A and B are parameters which depend on the value of S(Q,t) at long times.[62] As shown in Figure 9, the obtained result is by no means trivial. The KWW functional form does not accurately describe all the experimental spectra. Surprisingly, the experimental observations can not be described by a single monoexponential decay (or only one τ parameter), indicating that more than one dynamics was observed. Considering that a change in the neutron phase was also observed during the NSE experiments, one can assume that in addition to proton dynamics, magnetic fluctuations were also observed. Paradoxically, and as proven below, the implicit polarization analysis of the NSE technique, directed us to identify Fe^{3+} fluctuations, which to date have never been taken into account on the determination of diffusion constants of water in clays!

Magnetic Measurements. After the NSE observation we were led to perform magnetic susceptibility measurements in both halloysite and montmorillonite clays. Bulk characterization of both samples show essentially identical behavior. As shown in Figure 10, the inverse susceptibility for montmorillonite follows a Curie−Weiss law, $\chi = C/(T - \Theta)$. The obtained effective Bohr magneton number per iron ion of 5.0 μ_B is comparable with other analogous systems.[63,64] If the iron in a silicate is sufficiently dilute, magnetic exchange interactions, which tend to align the moments of neighboring cations parallel or antiparallel, may be neglected. In the present case, the existence of antiferromagnetic correlations between Fe^{3+} centers in montmorillonite is indicated by the decreasing nature of χT vs T [see the inset of Figure 10].[35] However, from our measurements in the hydrated clays, we infer that the iron content does not exceed the "percolation threshold" as long-range magnetic ordering was not observed.

We must remember that the Q-dependence of the magnetic neutron scattering cross section of a single magnetic ion and the variation of the component characterizing the scattering law for diffusion both give a substantial contribution in the same Q-region (see Figure 2). Therefore, any evaluation of diffusivity parameters, including the ones described in this manuscript, must be now accepted with extreme caution and, the previous differences obtained from the analyses of ToF and spin−echo data may be related to such spin correlation; i.e., the up to date evaluated $D_{apparent}$ may have been expressed as follows: $D_{apparent} = D_{water} + D_{magnetic}$, where $D_{magnetic}$ is related to the spin diffusion coefficient, which is described in terms of the spin−spin relaxation time.[65]

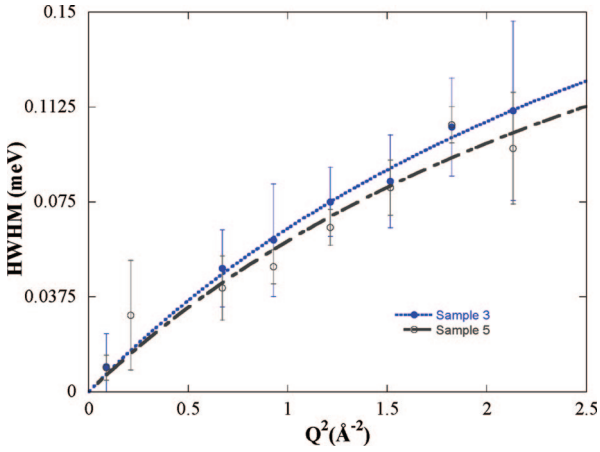

Figure 8. Line-width (HWHM) as a function of Q^2 of the QE component for water contained in the Halloysite (sample 3, ●) and Montmorillonite (sample 5, ○) without interlayer water using PG002, with $\Delta E = 25$ μeV. The solid lines are fit to the data using the jump diffusion model giving a diffusion constant value and average residence time very similar to bulk water.

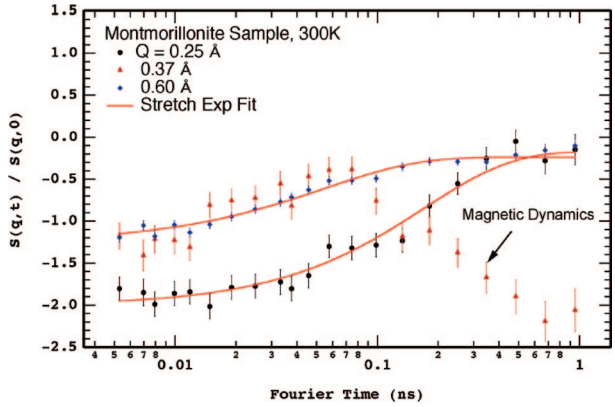

Figure 9. Q resolved $S(Q,t)$ scans of the montmorillonite sample at 300K for $Q = 0.25$, 0.37, and 0.6 Å^{-1}. Fits of the experimental data with stretched exponential KWW functions (solid line) are also shown. The clear deviation can be related to the magnetic scattering.

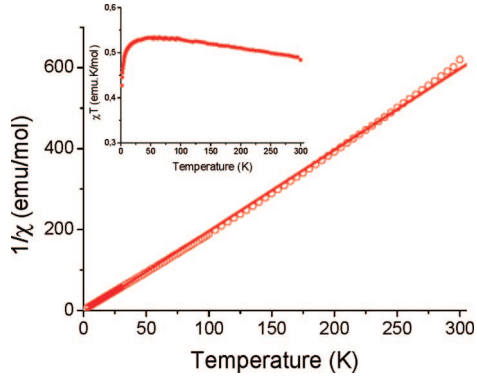

Figure 10. Inverse mass susceptibility versus T of montmorillonite measured at 1 kOe. The inset of the figure χT vs T gives further evidence of antiferromagnetic correlations between the Fe^{3+} ions.

Conclusions

The interaction of water with clays has been the subject of numerous papers of importance to such diverse fields as; agriculture, oil drilling, molds in the iron industry, pharmaceuticals and adhesives. Here it has been shown that, depending on the time range of the motion (type of water observed in the spectral window given by the spectrometer), the correlation between translational and rotational diffusion of interlayer water in halloysite and montmorillonite can be interpreted using either the Sears expansion or the "relaxing cage model".

Before using neutron scattering to give a final answer to questions such as whether the cation or the surface plays the major role in the water mobility, the following factors have to be explicitly taken into account: (1) allowance for correlation between the translational and rotational movement of water, (2) allowance for the different range of diffusion of waters in clays, (3) ensuring that the chosen time range (determined by the resolution of the QENS instrument) matches the expected ranges of diffusion, and (4) allowing for correction of the magnetic scattering contribution.

Using QENS at room temperature it has been shown that for the same hydration level (a monolayer of water in the interlayer space) the water diffusion coefficient in halloysite is similar to that of montmorillonite. An extension of water behavior in montmorillonite to lower temperatures than in halloysite was shown from EFW results. Thus, analogous to the behavior observed in organic membranes it seems that the interlayer Na^+ ions would balance the difference between the interlayer surfaces and facilitate the water mobility.

The NSE and SQUID results presented here have given evidence for the existence of paramagnetic fluctuations in halloysite and montmorillonite and confirm the truism that a standard neutron experiment measures total scattering which can be due to the coherent, the incoherent or the magnetic parts of the scattering. Considering that[66] the Q-dependence of magnetic scattering is modulated by $f^2(Q)$, which decreases with increasing Q, and that the diffusion process is characterized by a Lorentzian width of DQ^2 the discrimination from magnetic scattering to water diffusion is complicated. It is therefore clear that, in natural clays containing magnetic ions incorporated in the structure, it will be difficult to assess *real time* characteristics of water diffusion without polarization analysis. Even though magnetic scattering is important, and the obtained diffusion coefficients must be seen as *apparent values*, the work presented here allows us to conclude that there are differences between interlayer water in montmorillonite, interlayer water in halloysite, and surface water on the clay.

Finally, we suggest that the difference between the QENS and NSE results reported earlier could be due to either of two effects: that the effect of magnetic scattering was not allowed for, and or that different resolution windows measure different diffusivities. In conclusion, and as pointed out by Hecht and Geissler[67] almost 40 years ago, results from natural clays can be difficult to interpret and it would be easier to work with synthetic clays, which have the double advantage of not possessing structural protons, since the hydroxyl are replaced by fluorine, and of containing a smaller concentration of paramagnetic ions.

Acknowledgment. H.N.B. and L.P.A. thank N. Malikova and H. Schober for discussions. We acknowledge the support of the ISIS Facility and of the ILL in providing the neutron research facilities used in this work. Financial support was given by the *Access to Major Research Facilities Programme*, part of the *International Science Linkages Programme,* established under the Australian Government's innovation statement, *Backing Australia's Ability*. L.P.A. acknowledges the travelling support funding from D. H. Aldridge.

References and Notes

(1) Damme, H. V.; Gmira, A. In *Handbook of Clay Science*; Bergaya, F., Theng, B. K. G., Lagaly, G., Eds.; Elsevier: Amsterdam, 2006; pp 1113–1127.

(2) Swenson, J.; Bergman, R.; Howells, W. S. *J. Chem. Phys.* **2000**, *113*, 2873.
(3) North, F. K. *Petroleum Geology*; Unwin-Hyman: Boston, MA, 1990.
(4) Williams, L. B.; Canfield, B.; Voglesonger, K. M.; John, R *Geology* **2005**, *33*, 913.
(5) Brack, A. In *Handbook of Clay Science*; Bergaya, F., Theng, B. K. G., Lagaly, G., Eds.; Elsevier: Amsterdam, 2006; pp 379−389..
(6) Farmer, V. C.; Russell, J. D. *Spectrochim. Acta* **1964**, *20*, 1149.
(7) Farmer, V. C.; Russell, J. D. *Clays Clay Miner.* **1967**, *15*, 121.
(8) Mooney, R. W.; Keenan, A. C.; Wood, L. A. *J. Am. Chem. Soc.* **1952**, *74*, 1367.
(9) Cebula, D. J.; Thomas, R. K.; White, J. W. *Clays Clays Miner.* **1981**, *29*, 241.
(10) Kamitakahara, W. A.; Wada, N. *Mol. Cryst. Liq. Cryst* **2000**, *341*, 503.
(11) Malikova, N.; Cadene, A.; Dubois, E.; Turq, P. *J. Phys. Chem. B* **2006**, *110*, 3206.
(12) Swenson, J.; Bergman, R.; Longeville, S. *J. Chem. Phys.* **2001**, *115*, 11299.
(13) Swenson, J.; Bergman, R.; Bowron, D. T.; Longeville, S. *Philos. Mag. B* **2002**, *82*, 497.
(14) Bergman, R.; Swenson, J.; Börjesson, L.; Jacobsson, P. *J. Chem. Phys.* **2000**, *113*, 357.
(15) Kaviratna, P. D.; Pinnavaia, T. J.; Schroeder, P. A. *J. Phys. Chem. Solids* **1996**, *57*, 1897.
(16) Cruz, M. I.; Letellier, M.; Fripiat, J. J. *J. Chem. Phys.* **1978**, *69*, 2018.
(17) Churchman, G. J; Carr, R. M. *Clays Clay Miner.* **1975**, *23*, 382–388.
(18) Joussein, E.; Petit, S.; Churchman, J.; Theng, B.; Righi, D.; Delvaux, B. *Clays Clay Miner. 1* **2005**, *40*, 383.
(19) Pusch, R. In *Handbook of Clay Science*; Bergaya, F., Theng, B. K. G., Lagaly, G., Eds.; Elsevier: Amsterdam, 2006; pp 703−741.
(20) Bourg, I. C.; Sposito, G.; Bourg, A. C. M. *Clays Clay Miner.* **2006**, *54*, 363.
(21) Komadel, P.; Madejova, J.; Bujdak, J. *Clays Clay Miner.* **2005**, *53*, 313.
(22) Jaynes, W. F.; Bingham, J. M. *Clays Clay Miner.* **1987**, *35*, 440.
(23) Johnston, C. T.; Sposito, G.; Erickson, C. *Clays Clay Miner.* **1992**, *40*, 722.
(24) Xu, W.; Johnston, C. T.; Parker, P.; Agnew, S. F. *Clays Clay Miner.* **2000**, *48*, 120.
(25) Low, P. F. In *Advances in Agronomy*; Norman, A. G., Ed.; Academic Press: New York, 1961; Vol. 13.
(26) Churchman, G. J.; Aldridge, L. P.; Carr, R. M. *Clays Clay Miner.* **1972**, *20*, 241.
(27) Komadel, P.; Madejova, J.; Bujdak, J. *Clays Clay Miner.* **2005**, *53*, 313.
(28) Telling, M. T. F.; Andersen, K. H. *Phys. Chem. Chem. Phys.* **2005**, *7*, 1255.
(29) Lovensy, S. W. In *Theory of Neutron Scattering from Condensed Matter*; Oxford University Press: Oxford, U.K., 1984.
(30) Bée, M. In *Quasielastic Neutron Scattering: Principles and Applications in Solid State Chemistry, Biology and Materials Science*: Adam Hilger: Bristol, U.K., 1988.
(31) Cook, J. C.; Petry, W.; Heidemann, A.; Barthélemy, J.-F. *Nucl. Instr. and Meth.* **1992**, *A312*, 553.
(32) Malikova, N.; Cadene, A.; Marry, V.; Dubois, E.; Turq, P.; Zanotti, J.-M.; Longeville, S. *Chem. Phys.* **2005**, *317*, 226.
(33) Malikova, N.; Cadene, A.; Dubois, E.; Marry, V.; Durand-Vidal, S.; Turq, P.; Breu, J.; Longeville, S.; Zanotti, J.-M. *J. Phys. Chem. B* **2007**, *111*, 17603.
(34) Brown, C. M.; A Manson, J. L. *J. Am. Chem. Soc.* **2002**, *124*, 12600.
(35) Bordallo, H. N.; Chapon, L.; Manson, J. L.; Hernandez-Velasco, J.; Ravot, D.; Reiff, W. M.; Argyriou, D. N. *Phys. Rev. B* **2004**, *69*, 224405.
(36) Brown, P. J. In *International Tables for Crystallography*; Prince, E., Ed.; Kluwer Academic Publishers: Amsterdam, 2004; *Vol. C, Magnetic form factors*, Chapter 4.4.5, pp 391−399.
(37) M. Baioumy, M.; Hassan, M. S. *Clay Miner.* **2004**, *39*, 207.
(38) Bordallo, H. N.; Aldridge, L. P.; Desmedt, A. *J. Phys. Chem. B* **2006**, *110*, 17966.
(39) Aldridge, L. P.; Bordallo, H. N.; Desmedt, A. *Physica B* **2004**, *350*, e565.
(40) Hempelmann, R. In *Quasi-Elastic Neutron Scattering and Sold State Diffusion*; Oxford University Press Inc.: New York, 2000.
(41) Zanotti, J.-M.; Bellissent-Funel, M.-C.; Chen, S.-H. *Europhys. Lett.* **2005**, *71*, 91.
(42) Ertl, G.; Knözinger, H. and Weitkamp, J. In *Preparation of Solid Catalysts*: Wiley-VCH: New York, 1999.
(43) Kamitakahara, W.; Wada, N. *Phys Rev. E* **2008**, *77*, 41503.
(44) Chakrabarty, D.; Gautam, S.; Mitra, S.; Gil, A.; Vicente, M. A.; Mukhopadhyay, R. *Chem. Phys. Lett.* **2006**, *426*, 296.
(45) Mamontov, E. *J. Chem. Phys.* **2005**, *123*, 24706.
(46) Bordallo, H. N.; Herwig, K. W.; Luther, B. M.; Levinger, N. E. *J. Chem. Phys.* **2004**, *121*, 12457.
(47) Teixeira, J.; Bellissent-Funel, M. C.; Chen, S. H.; Dianoux, A. J. *Phys. Rev. A* **1985**, *31*, 1913.
(48) Sears, V. F. *Can. J. Phys.* **1966**, *44*, 1299.
(49) Singwi, K. S.; Sjölander, A. *Phys. Rev.* **1960**, *119*, 863.
(50) Chen, S. -H.; Gallo, P.; Sciortino, F.; Tartaglia, P. *Phys. Rev. E* **1997**, *56*, 4231.
(51) Zanotti, J. -M.; Bellissent-Funel, M. -C.; Chen, S. -H. *Phys. Rev. E* **1999**, *59*, 3084.
(52) Swenson, J.; Jansson, H.; Howells, W. S.; Longeville, S. *J. Chem. Phys.* **2005**, *122*, 84505.
(53) The analysis was performed using the routines available in the program Fitmo. For details see: Fitter, J. *User Manual for FITMO (NEAT TOF-Data Analysing Programm)*; HMI: Berlin, 1997.
(54) The analysis was performed using the routines available in the program MODES. For details see: Howells, W. S. *Technical Report, Rutherford Appleton Laboratory, RAL-TR-96−006*; **1996**.
(55) Marry, V.; Turq, P.; Cartailler, T.; Levesque, D. *J. Chem. Phys.* **2002**, *117*, 3454.
(56) Chang, F.-R.; Skipper, N.; Sposito, G. *Langmuir* **1995**, *11*, 2734.
(57) Chang, F.-R.; Skipper, N.; Sposito, G. *Langmuir* **1997**, *13*, 2074.
(58) Chang, F.-R.; Skipper, N.; Sposito, G. *Langmuir* **1998**, *14*, 1201.
(59) Sutton, R.; Sposito, G. *J. Colloid Interface Sci.* **2001**, *237*, 174.
(60) Gay-Duchosal, M.; Powell, D. H.; Lechner, R. E.; Ruffle, B. *Phys. B: Condens. Matter* **2000**, *276−278*, 234.
(61) Nair, S.; Chowdhuri, Z.; Peral, I.; Neumann, D. A.; Dickinson, L. C.; Tompsett, G.; Jeong, H-K.; Tsapatsis, M. *Phys. Rev. B* **2005**, *71*, 104301.
(62) The variation of β from unity would indicate that the dynamics observed has a wide distribution of relaxation times.
(63) Ballet, O.; Coey, J. M. D.; Mangin, P.; Townsend, M G. *Solid State Commun.* **1985**, *155*, 787.
(64) Ballet, O.; Coey, J. M. D. *Phys Chem Miner.* **1982**, *8*, 218.
(65) Bernier, P; Alloul, H J. *Phys. F: Metal Phys.* **1976**, *6*, 1193.
(66) Plakhtii, V. P.; Golosovskii, I. V.; Bedrisova, M. N.; Smirnov, O. P.; Sokolov, V. I.; Mill, B. V.; Parfenova, N. N. *Phys. Stat. Solidi (a)* **1977**, *39*, 683.
(67) Hecht, A. M.; Geissler, E. *Spec. Discuss. Faraday Soc.* **1970**, *1*, 210.

JP803274J